JACS
JOURNAL OF THE AMERICAN CHEMICAL SOCIETY

ARTICLE

pubs.acs.org/JACS

Transmetalation of Methyl Groups Supported by Pt^{II}—Au^{I} Bonds in the Gas Phase, in Silico, and in Solution

Daniel Serra, Marc-Etienne Moret, and Peter Chen*

Laboratorium fur Organische Chemie, Eidgenössische Technische Hochschule ETH Zurich, Wolfgang-Pauli-Strasse 10, Zurich CH-8093, Switzerland

Supporting Information

ABSTRACT: We report Pt^{II}-to-Au^{I} methyl transfer reactions that occur in the gas phase and in solution. The heterobimetallic Pt^{II}/Au^{I} complexes $\{[(dmpe)PtMe_2][AuPR_3]\}^+$ (R = Me (**2a**), Ph (**2b**), ^{t}Bu (**2c**)), observed in the gas phase by means of electrospray ionization, were subjected to collision induced dissociation (CID) from which we could observe Pt-to-Au transmetalation along two reaction pathways involving formation of a Au—Me bond, analogous to those observed for the Pt^{II}/Cu^{I} complex recently reported. In the first pathway, neutral AuMe is generated with concomitant migration of PR_3 from Au^{I} to the Pt^{II} center, forming cation $[(dmpe)PtMe(PR_3)]^+$ (R = Me (**5a**) or Ph (**5b**)). In the second pathway, the monophosphine stays attached to the gold center, yielding cation $[(dmpe)PtMe]^+$ (**7**) and R_3PAuMe. Quantitative energy-resolved collision induced dissociation experiments as well as density functional theory (DFT) calculations were used to investigate the potential surface involved in the transmetalation processes. Energy barriers of 22.3 and 47.9 kcal mol^{-1} for the two reaction processes of **2b** and of 45.4 kcal mol^{-1} for the single reaction process of **2c** were obtained. Parallel reactivity is observed in THF solution, allowing for a comparison of the product distributions with those observed in the gas phase, and the postulation of simple steric control of the branching ratio between the two pathways. DFT calculations at the M06-2X//BP86/TZP level were in good agreement with the experiments.

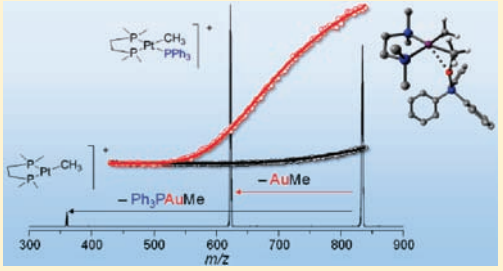

INTRODUCTION

The transmetalation of alkyl or aryl functionalities between two different metal centers is a fundamental process invoked in many cross-coupling reactions catalyzed by late transition metal[1] such as, for example, the alkynyl ligand transfer from Cu(I) to Pd(II) involved in the copper-cocatalyzed Sonogashira process, which provides arylacetylenes or enynes.[1d,2]

Although the abundant occurrences of transmetalation reactions are well established in coupling processes, studies on the detailed mechanism of the step itself are uncommon. Determination of mechanistic information, such as the quantitative thermochemistry, is then crucial in order to improve catalyst design, particularly when attempting to couple catalytic cycles involving two different metals. With the ultimate goal to functionalize hydrocarbons catalytically, we focus our attention on the use of heterobimetallic systems that can work cooperatively: each metal can perform a different task for which it is optimal, leading to novel or improved activity. Systems involving square planar d^8 and electrophilic d^{10} metal centers are prone to form dative metal—metal bonds, which are observed in a wide range of heterobimetallic complexes, including Rh^{I}/Ag^{I},[4a,b] Ir^{I}/Ag^{I},[4a,b] Ir^{I}/Au^{I},[4c−e] Ir^{I}/Cu^{I},[4b] Rh^{I}/Cu^{I},[4b] Pd^{II}/Ag^{I},[4f,g] Pd^{II}/Au^{I},[4h] Pd^{II}/Hg^{II},[4i,k] Pt^{II}/Cd^{II},[4l] Pt^{II}/Hg^{II},[4i,j] Pt^{II}/Ag^{I},[4h,m] and Pt^{II}/Cu^{I}.[4h,m] Indeed the close proximity of the two metals is a crucial condition to observe the transmetalation process for which the organic group is transferred as for example in the recently reported[5] system $\{[(dmpe)PtMe_2]Cu(PMe_3)\}^+$ or in the case of $AgBF_4$ which catalyzes a fast methyl scrambling in $[(2,2'\text{-bpy})PtMe_2]$.[6]

Gas-phase reactivity studies using electrospray ionization tandem mass spectrometry (ESI-MS/MS) techniques have given useful mechanistic information about fundamental catalytic processes[7,9] such as olefin metathesis,[8a] cyclopropanation,[8b,f] reductive elimination,[8c] C—H bond activation.[8d,e] Having successfully applied this method to methyl group trzansmetalation in a Pt^{II}/Cu^{I} system[5] (Figure 1), we are now motivated to obtain more detailed insights into the factors controlling the transmetalation reaction by varying the coinage metal and the phosphine ligands. Herein we report experimental results in the gas phase for related Pt^{II}/Au^{I} systems, which clearly demonstrate that (i) the transmetalation of a methyl group from Pt(II) to Au(I) proceeds *via* a heterobimetallic cationic complex intermediate, (ii) two competitive reaction pathways can occur in analogy to the Pt^{II}/Cu^{I} system, and (iii) steric hindrance can be used to control the branching ratio between competing transmetalation pathways. We determined the energy barriers for the transmetalation reactions by quantitative collision-induced dissociation (CID) threshold measurements for two systems, which were compared with activation energies obtained from DFT calculations. Remarkably experiments in solution demonstrate that the transmetalation processes are also occurring in the condensed

Received: December 1, 2010
Published: May 11, 2011

dx.doi.org/10.1021/ja110405q | J. Am. Chem. Soc. 2011, 133, 8914–8926

phase, generating products similar to those observed in the gas phase, with the branching ratio between product channels in solution following the same trends as observed in the gas phase.

RESULTS AND DISCUSSION

Gas-Phase Study. In this work a strong chelating ligand bis(dimethylphosphino)ethane (dmpe) was used to stabilize the dimethyl-platinum(II) fragment, and the stabilizing ligand on gold was varied to probe steric and electronic effects on the transmetalation processes. Phosphine−gold chloride complexes R_3PAuCl (R = Me, Ph, ^{t}Bu) were reacted in acetonitrile with an equimolar amount of $[(dmpe)PtMe_2]$ (**1**)[10] after *in situ* halide abstraction using one equivalent of NaOTf (Scheme 1). In our ESI-MS experiment NaOTf was chosen as a weak abstracting agent so that the transmetalation reactions do not proceed to completion prior to the electrospray. Under these conditions **1**, R_3PAuCl, and NaOTf are most likely present simultaneously in the solution, generating a small steady-state concentration of the bimetallic complexes during the spray. The reaction mixtures were further diluted with acetonitrile and electrosprayed on a Thermo Finnigan TSQ Quantum instrument, which allowed the observation of small signals for the heterobimetallic cations **2a**−**c**, as identified by their m/z ratios (648, 834 and 774, respectively), isotope patterns and their characteristic collision-induced fragmentation behavior (Scheme 2). Notably, cations **2a** and **2b** were found to be unstable and already undergo a fast transmetalation process while preparing the solutions at low temperature (∼−30 °C), as indicated by the high intensity of the peaks for product ions **5a** and **5b** at m/z 436 and 622, respectively, in the ESI-MS spectra (see the Supporting Information).

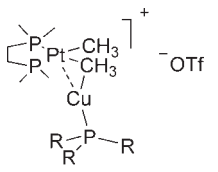

Figure 1. Previously reported Pt^{II}−Cu^{I} systems.

Scheme 1. Generation of Ions 2a−c

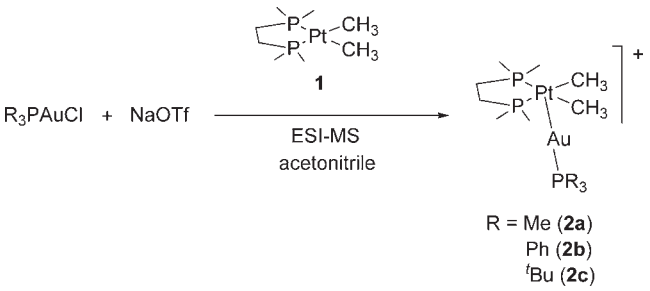

Analogous to the isoelectronic Pt^{II}/Cu^{I} system,[5] after mass selection of **2a** and **2b** each undergo two competing reactions upon collision-induced dissociation (CID) (Figure 2A, B), involving the transfer of a methyl group from Pt(II) to Au(I) (Scheme 2). In process (I), the methyl group transmetalation occurs with simultaneous migration of the monophosphine ligand from Au(I) to Pt(II) giving rise to the observed $[(dmpe)PtMe(PR_3)]^+$ cation **5a**/**b** (R = Me, Ph) along with the neutral methylgold(I). Conversely, in process (II) migration of the monophosphine does not occur and thus the coordinatively unsaturated complex $[(dmpe)PtMe]^+$ (**7**)[11] is produced as the observable cation, along with the neutral R_3PAuMe (R = Me, Ph).

In the case of cation **2c** ($R = {}^t$Bu), mass selection of the parent signal followed by CID leads exclusively to reaction (II), **2c** → **7** + $(^t Bu)_3PAuMe$ (Figure 2C). The first pathway is presumably hampered by the steric demands of the tris-(*tert*-butyl)phosphine supporting ligand, which should disfavor the formation of cation **5c**. In contrast to the Pt^{II}/Cu^{I} systems,[5] the Pt^{II}/Au^{I} heterobimetallic cations react more cleanly, showing only transmetalation reaction channels. They did not undergo Pt−Au or Au−P bond dissociation which would lead to additional reaction channels (see the Supporting Information).

CID Threshold Measurements. Determination of CID thresholds requires that the intensity of the parent ion remains sufficient over several hours, which is an issue of sample preparation. Therefore, to allow measurement of the more reactive systems, freshly prepared acetonitrile solutions of R_3PAu^+ (R = Me, Ph) and of complex **1** were mixed at −5 °C in a FlowStart microreactor equipped with an ultrafast mixing chip connected to the spray head of our spectrometer (see the Supporting Information). Unfortunately, **2a** was too reactive to allow measurements even with this sample introduction technique.

Energy-resolved reaction cross sections were recorded on a customized Finnigan MAT TSQ-700 spectrometer as previously described.[8c] The generated cation **2b** was collided with 30−110 μTorr argon to monitor simultaneously the two competing transmetalation reactions, leading to **5b** and AuMe versus **7** and Ph_3PAuMe. The experimental reaction cross section curves for both processes were extrapolated to zero pressure to impose strict single-collision conditions, and fitted with L-CID[12] (Figure 3). As discussed previously,[12] some

Scheme 2. Collision Induced Dissociation (CID) Reactions Observed for Cations 2a−c

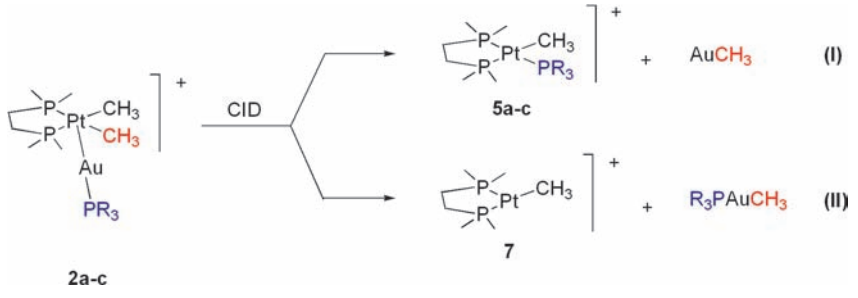

dx.doi.org/10.1021/ja110405q | J. Am. Chem. Soc. 2011, 133, 8914–8926

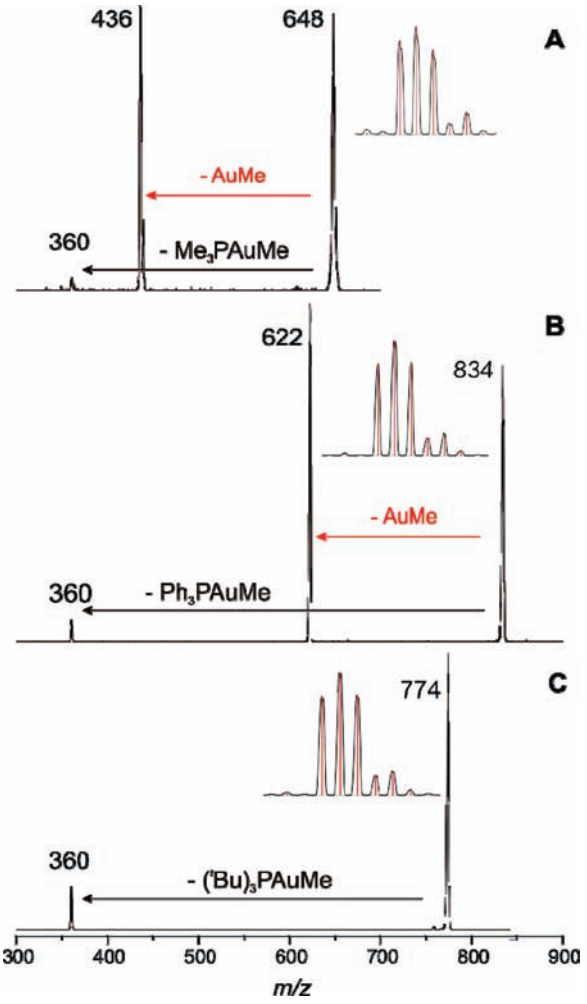

Figure 2. CID spectra of **A**) $\{[(dmpe)PtMe_2]Au(PMe_3)\}^+$ (**2a**, m/z = 648), **B**) $\{[(dmpe)PtMe_2]Au(PPh_3)\}^+$ (**2b**, m/z = 834), and **C**) $\{[(dmpe)PtMe_2]AuP(^tBu)_3\}^+$ (**2c**, m/z = 774) obtained at 50 V collision offset with 0.2 mTorr argon in the collision cell. Product peak assignment: m/z 436 $[(dmpe)Pt(Me)(PMe_3)]^+$ (**5a**), 622 $[(dmpe)Pt(Me)(PPh_3)]^+$ (**5b**), and 360 $[(dmpe)Pt(Me)]^+$ (**7**). (Insets) Experimental (black) and calculated (red) isotope patterns of complexes **2a**−**c**.

information on the nature of the transition state (TS) is necessary for an appropriate treatment of the kinetic shift. A "tight" transition state model should be used when the rate-limiting step is an intramolecular rearrangement, while a "loose" TS model applies when the rate-limiting step is a dissociation without reverse activation barrier. The distinction arises from the fact that the rovibrational density of states of a tight transition state closely resembles that of the parent ion (for a large enough complex), while a loose transition state is best viewed as two loosely bound, orbiting fragments and therefore possesses a much larger density of states. Chemical intuition,[13] confirmed by DFT calculations, indicated that reaction (I) is best described by a tight[14] TS model (*vide infra*), whereas a loose TS model should be used for reaction (II). Therefore two-channel L-CID fits were performed accordingly, affording energy barriers of 22.3 ± 0.9 kcal mol^{-1} for reaction channel (I) (tight), and 47.9 ± 1.8 kcal mol^{-1} for reaction channel (II) (loose) (Figure 3, Table 1).

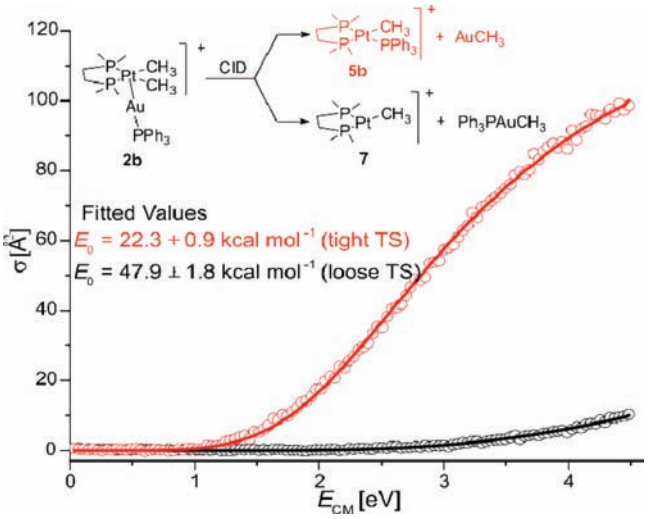

Figure 3. Zero-pressure extrapolated reactive cross sections (circles) and L-CID fits (lines) as functions of center-of-mass collision energy for the CID reactions **2b** → **5b** + AuMe (red) and **2b** → **7** + Ph_3PAuMe (black).

In a similar fashion we performed CID threshold measurements for the methyl group transmetalation in the heterobimetallic cation **2c**, involving the more sterically hindered tris-(*tert*-butyl)phosphine as supporting ligand on gold, which afforded a single reaction channel. Figure 4 shows the zero-pressure extrapolated cross section curve and the L-CID fit, which provided a barrier of 45.4 ± 1.6 kcal mol^{-1}, assuming that a loose transition-state model also applies for this process (Table 1).

DFT Calculations. A detailed investigation of the systems **2a**−**c** was performed by means of density functional theory (DFT) calculations in order to illuminate the mechanisms of the two distinct transmetalation pathways. The involved intermediates and transition states were located at the BP86/6-31G(d,p); Pt,Au:SDD level of theory.[15,16] Subsequently, three density functionals were considered for single-point energy evaluations: mPW1K[17] the modified Perdew−Wang one-parameter hybrid developed for kinetics, which was successfully employed for several transition-metal systems;[5,18−20]M06-L,[21−23] which was designed to model main-group and transition-metal thermochemistry, kinetics, and noncovalent interactions; and the M06-2X[23,24] functional, which was intended for main-group thermochemistry, kinetics and nonbonding interactions because of its large fraction of Hartree−Fock exchange. Table 2 lists the relative energies for the considered density functionals for the intermediates and transition states (TS) involved in reaction channels (I) and (II). Figure 5 presents the potential energy diagram for both reaction channels, which is based on the calculated energies obtained with the M06-2X density functional. Included in the diagram are the optimized geometries of the intermediates and transition states originating from the bimetallic complex **2a**.

As shown in Figure 5 (left), reaction channel (I) involves the initial formation of a Pt−Au methyl bridged intermediate **3**, which undergoes a migration of the CH_3−Au−P fragment from one side of the coordination plane of Pt to the other, forming intermediate **4** *via* a transition state $\mathbf{TS_{3-4}}$. In this TS a Au−P bond is partially broken and a Pt−P bond is partially formed,

dx.doi.org/10.1021/ja110405q |*J. Am. Chem. Soc.* 2011, 133, 8914–8926

Table 1. L-CID Fitting Results (kcal mol^{-1}) for the CID Reactions 2b → 5b + AuMe, 2b → 7 + Ph_3PAuMe, and 2c → 7 + $(^tBu)_3PAuMe$

Process	Channel	TS model assumption[a]	E_0
2b → 5b + AuMe	(I)	Tight[b]	22.3(9) [c]
2b → 7 + Ph_3PAuMe	(II)	Loose	47.9(18) [c]
2c → 7 + $(^tBu)_3PAuMe$	(II)	Loose	45.4(16)

[a] Based on DFT calculation. [b] The L-CID fitting using a Loose TS model is described in the Supporting Information. [c] Two-channel fits.

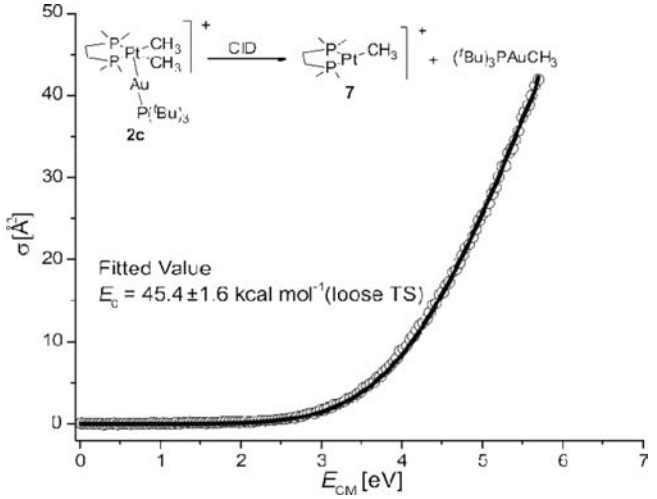

Figure 4. Zero-pressure extrapolated reactive cross sections (circles) and L-CID fit (line) as functions of center-of-mass collision energy for the CID reaction **2c** → **7** + $(^tBu)_3PAuMe$.

suggesting that the concerted movement of the gold−phosphine moiety is the presumed reason for the tight character of the TS. Pt−Au bond dissociation from **4** finally leads to the observed cationic complex **5** and neutral AuMe.

At the M06-L level of theory markedly lower-energy barriers for the transmetalation step are calculated for process (I) ($\mathbf{TS_{3-4}}$, Table 2), suggesting that the loose product dissociation should be rate determining throughout the scanned collision energy range. However, fitting of both reaction cross sections of **2b** with a loose TS model afforded an experimental barrier of 36.8 kcal mol^{-1} for process (I), which is 15.6 kcal mol^{-1} higher than the calculated M06-L dissociation energy of 21.2 kcal mol^{-1} (see the Supporting Information for detail). We therefore conclude that the M06-L density functional underestimates the transmetalation barrier and consequently the process **2b** → **5b** + AuMe is not appropriately represented by a loose TS model, as it was also observed for the Pt^{II}−Cu^{I} system. In contrast, for mPW1K and M06-2X density functionals, the transition state $\mathbf{TS_{3-4}}$ and the subsequent dissociation step to **5a**−**c** + AuMe for reaction (I) are calculated to be similar in energy (with differences in favor of $\mathbf{TS_{3-4}}$ of 3.4 (**2a**), 0.9 (**2b**), and 1.0 kcal mol^{-1} (**2c**) for mPW1K, and of 4.4 (**2a**), 3.0 (**2b**), and 3.8 kcal mol^{-1} (**2c**) for M06-2X). The rate constant of the tight transmetalation process, *via* $\mathbf{TS_{3-4}}$, necessarily increases less rapidly with excess energy than that of the subsequent loose dissociation into **5** + AuMe because the density-of-states rises more slowly with energy for a tight transition state than it does for a loose one. Thus, even if the tight transition state were to lie slightly lower on the potential energy surface than the dissociation limit, the rate-determining step switches from the dissociation near threshold to the transmetalation at higher collision energies. A similar situation was recently reported by our group for reductive elimination from a palladium *N*-heterocyclic complex and it was found that a model with a tight transition state did indeed produce the better threshold energy.[8c] Indeed, the experimentally determined tight barrier of 22.3 kcal mol^{-1} (Table 2) for the conversion of **2b** into **5b** + AuMe is in good agreement with the calculated energy obtained with mPW1K and M06-2X (21.1 and 20.9 kcal mol^{-1}, respectively).

Table 2. Calculated Relative Energies (kcal mol^{-1}) for Reaction Channel (I) (2a−c → 5a−c + AuMe) (top) and Reaction (II) (2a−c → 7 + R_3PAuMe) (bottom) for the mPW1K, M06-L, and M06-2X Functionals, Evaluated with ADF[51] BP86/TZP Geometries

reaction (I)	system	2	3	$\mathbf{TS_{3-4}}$	4	5 + AuMe
mPW1K	a	0	−1.4	15.9	3.4	19.3
	b	0	−1.6	20.2	7.3	21.1
	c	0	−1.0	45.9	32.7	46.9
M06-L	a	0	1.2	9.4	−3.1	22.5
	b	0	1.5	9.4	−3.1	22.7
	c	0	3.0	31.4	18.7	44.8
M06-2X	a	0	1.0	16.7	3.4	21.1
	b	0	0.7	17.9	4.9	20.9
	c	0	0.2	43.1	30.1	46.9
reaction (II)	**system**	**2**	**3**	$\mathbf{TS_{3-6}}$	**6**	**7 + R_3PAuMe**
mPW1K	a	0	−1.4	12.2	2.9	33.8
	b	0	−1.2	13.3	4.1	36.2
	c	0	−1.0	13.8	4.0	36.4
M06-L	a	0	1.2	14.6	7.8	38.9
	b	0	1.5	17.3	10.3	42.3
	c	0	3.0	19.2	12.1	45.0
M06-2X	a	0	1.0	8.8	2.8	38.4
	b	0	0.7	10.0	3.8	41.3
	c	0	0.2	11.7	5.3	43.3

In the case of reaction channel (II) (Figure 5, right), intermediate **3** undergoes dissociation of the Pt−Au bond to form the methyl-bridged intermediate **6** *via* a relatively low energy transition state $\mathbf{TS_{3-6}}$, which involves a Pt−C−Au angle expansion around the groups to be transmetalated. Subsequent rupture of the Pt−C bond affords the observed product cation **7** along with the neutral R_3PAuMe complex. The DFT calculations indicate that the latter process is rate determining for all systems **2a**−**c** and functionals considered (Table 2). For all systems, the mPW1K density functional provides a dissociation energy that is notably lower than with

dx.doi.org/10.1021/ja110405q | *J. Am. Chem. Soc.* 2011, 133, 8914–8926

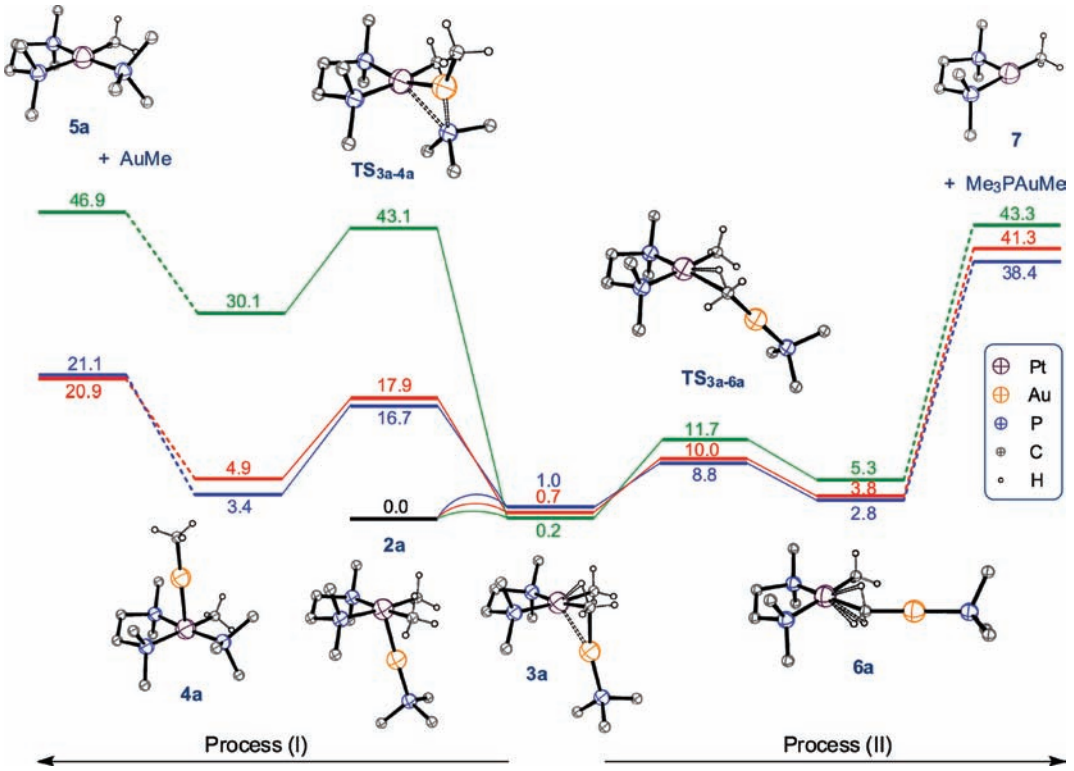

Figure 5. Calculated (M06-2X/TZP//BP86/6-31G(d,p);Pt,Au:SDD) potential energy surface for reaction process (I) (**2a**−**c** → **5a**−**c** + AuMe) and (II) (**2a**−**c** → **7** + R_3PAuMe) involving system **2a**, **2b**, and **2c**. Dashed lines indicate dissociations that proceed without a reverse activation barrier. For clarity only the structures involving system **2a** (BP86/6-31G(d,p);Pt,Au:SDD) are presented, and only the hydrogen atoms of the metal-methyl groups are shown. Energies represented (kcal mol^{-1}) are zero-point energy corrected.

either M06-L or M06-2X (by 4.6−6.9 kcal mol^{-1}). The experimentally determined barriers of 47.9 ± 1.8 kcal mol^{-1} (**2b** → **7** + Ph_3PAuMe) and 45.4 ± 1.6 kcal mol^{-1} (**2c** → **7** + (^{t}Bu)$_3$PAuMe) are reasonably well reproduced by the latter two density functionals, whereas mPW1K clearly underestimates the energy of these dissociations. M06-2X density functional demonstrates acceptable accuracy for both reaction channels involved, in contrast to M06-L and mPW1K, which are showing good accuracy either only in the case of a tight model (mPW1K) or only in the case of a loose model (M06-L).

It may at first appear surprising that reaction (I) is not observed for **2c** even though it is predicted to have a similar energetic barrier to reaction (II). However, one should take into account that, for two competing reaction channels having similar threshold energies but different transition state natures, the rate constant for a reaction with a loose transition state will be higher than that of a tight one because of the higher density of states of the former. This implies for competing channels with similar energetic barriers, the reaction over the loose transition state will proceed faster, even to the extent that the competing channel over a tight transition state will be unobservable experimentally.

The good performance of M06-2X may seem surprising, as it was originally intended for main group chemistry. Bimetallic transition metal systems may involve significant multireference character, to which a significant amount of static, near degeneracy, or nondynamical correlation energy is associated.[25] Since Hartree−Fock (HF) exchange improperly treats interelectron repulsions it is reasonable to say that hybrid functional with high HF contribution would lead to inaccuracies in the potential energy surfaces (PES). In order to evaluate the multireference character in our complexes, we employed the B_1 parameter as proposed by Truhlar and co-workers.[25−27] To this end, BLYP and B1LYP//BLYP dissociation energies were compared, providing B_1 values ranging from −2.7 to 11.8 kcal mol^{-1} (see the Supporting Information), which are comparable to the ∼10 kcal mol^{-1} values considered for single reference complexes. In our systems M06-2X is particularly efficient in describing both observed reaction channels presumably because the limited contribution from the d-orbitals of gold to the chemical bonding gives rise to substantially single reference character. Therefore the use of M06-2X for these transition metal systems can be regarded as legitimate.

Solution-Phase Study. To our knowledge only one Pt^{II}/Au^{I} complex, $\{[PtMe_2(2,2'\text{-bpy})](AuPPh_3)\}^+ X^-$ (bpy = bipyridine, X = NO_3, PF_6, BF_4), related to our systems, has been characterized by ^{31}P NMR spectroscopy.[28] Although it is a good candidate to study the methyl transfer between Pt(II) and Au(I) centers, this heterobimetallic complex was reported to exhibit no transmetalation reactivity. On the other hand, the methyl-for-chloride exchange between *cis*-$[PtMe_2(PMe_2Ph)_2]$ and $[ClAu(PMe_2Ph)]$, leading to *trans*-$[PtCl(Me)(PMe_2Ph)_2]$ and $[MeAu(PMe_2Ph)]$, has been reported to occur in solution.[29] It is believed to occur *via* a heterobimetallic intermediate which was neither isolated nor observed.

In this study, when complex **1** is reacted at room temperature with a stoichiometric amount of R_3PAuCl (R = Me,[30] Ph,[31] ^{t}Bu[32]) in THF-d_8 a clean reaction takes place leading exclusively to the formation of methyl substituted gold complexes R_3PAuMe and neutral [(dmpe)PtMeCl] complex **9** as the sole

Scheme 3. Reaction between 1 and R_3PAuMe (R = Me, Ph, ^{t}Bu)

Table 3. ^{31}P NMR Results Involving Systems A, B, and C Depending on the Abstracting Agent

entry	system	abstr. agent	T (°C)	reaction time	products observed	conversion (%)
1	**A**	–	25	3d	**9**	n.d.[a]
					1	
					Me_3PAuMe	
					Me_3PAuCl	
2	**B**	–	25	3d	**9**	n.d.[a]
					1	
					Ph_3PAuMe	
3	**C**	–	25	5d	**9**	64[b]
					1	
					$(^tBu)_3PAuMe$	
					$(^tBu)_3PAuCl$	
4	**A**	NaBArF	−35	10 min	**5a**	47[c]
					Me_3PAuMe	
					Me_3PAuCl	
					9	
5	**B**	NaBArF	−35	30 min	**5b**	52[c]
					Ph_3PAuMe	
					9	
6	**C**	NaBArF	−35	1 h	**9**	68
					$(^tBu)_3PAuMe$ $(^tBu)_3PAuCl$	
					1	
7	**A**	AgOTf	−80	<10 min[d,e]	**5a**	100
					Me_3PAuMe $[(dmpe)PtMe(NCMe)]^+$	
8	**B**	AgOTf	−80	<10 min[d,e]	**5b**	100
					Ph_3PAuMe $[(dmpe)PtMe(NCMe)]^+$	
9	**C**	AgOTf	−80	<10 min[d]	$(^tBu)_3PAuMe$ $[(dmpe)PtMe(NCMe)]^+$	100

[a] The conversion could not be determined because of the poor solubility of R_3PAuCl (R = Me, Ph) in THF-d_8. [b] Based on the ratios of the ^{31}P NMR signals of $(^tBu)_3PAuMe$ and $(^tBu)_3PAuCl$ at the end of the reaction. [c] Yields of the isolated complex **5a** and **5b**: process (I) only. [d] The NMR tube was prepared and brought to the NMR spectrometer at −100 °C. The sample was inserted in a spectrometer set at −95 °C and stabilized to −80 °C in about 10 min. [e] The reaction takes place at −100 °C upon slow addition of a THF-d_8 solution of complex **1**, since a fast change of color is observed.

transmetalation products (Scheme 3). Complex **9** has been previously characterized and was synthesized for comparison purposes.[33]

Monitoring of the reaction by ^{31}P NMR (see the Supporting Information) reveals that the reactions progresses slowly, with both the precursors and transmetalation products being observed simultaneously as the reactions proceed over days,[34] this behavior being presumably due to a slow ionization of the gold precursors, followed by a much faster transmetalation once the bimetallic intermediate is formed. Because of the poor solubility of the R_3PAuCl (R = Me, Ph) precursors in THF and the low stability of the formed R_3PAuMe products (R = Me, Ph), quantitative determination of the reaction yields could be obtained only for the system involving the more stable $(^tBu)_3PAuMe$. Under these reaction conditions 64% of the gold−methyl complex was obtained after 5 days (Table 3, entry 3). The transmetalation products R_3PAuMe (R = Me,[35] Ph,[36] ^{t}Bu[37]) and [(dmpe)PtMeCl] obtained during our reactions at room temperature are analogous to the ones observed by Puddephatt et al.,[29] our reactions being different only by the fact that slower reactions processes are observed and that no equilibria are taking place (see the Supporting Information).

For a better comparison with the gas-phase results (*vide supra*), the reactions were performed in THF-d_8 in the presence of a chloride abstracting agent to ensure that cationic species are involved. Two abstracting agents, NaBArF (BArF = tetrakis(pentafluorophenyl)borate) and AgOTf were considered[38] and the general outcome of the reactions is described in Scheme 4 and 5, while the conditions and observed products are presented in Table 3. Systems **A**−**C** are defined as the reaction mixtures involving complex **1**, precursors R_3PAuCl (**A**: R = Me, **B**: R = Ph, **C**: R = ^{t}Bu), with or without halide abstracting agent.

System **A**−**C** can engage in two competing reaction pathways as described in Scheme 5, the first one (I) producing the

dx.doi.org/10.1021/ja110405q | *J. Am. Chem. Soc.* 2011, 133, 8914–8926

Scheme 4. Solution-Phase Products Observed Resulting from the Transmetalation Reactions (I) and (II)[a]

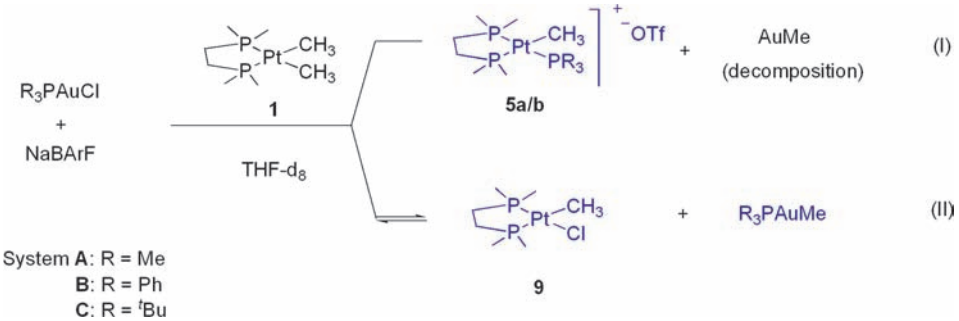

[a] The compounds with blue structures (**5a**, **5b**, **9**, and R_3PAuMe (R = Me, Ph, ^{t}Bu) were observed experimentally.

Scheme 5. Solution-Phase Products Observed Resulting from the Transmetalation Reactions (I) and (II)[a]

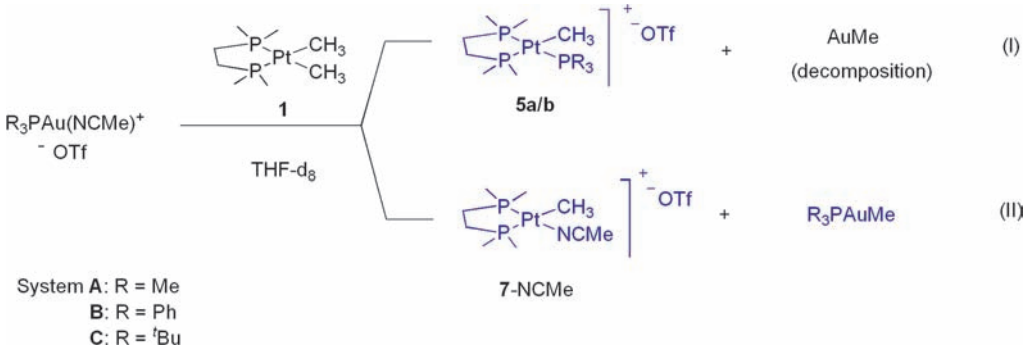

[a] The compounds with blue structures (**5a**, **5b**, 7-NCMe, and R_3PAuMe (R = Me, Ph, ^{t}Bu)) were observed experimentally.

observed complexes **5a**/**b** and the second one (II) generating the solvent adduct 7-NCMe or complex **9** and R_3PAuMe. Our ^{31}P NMR experiments did not show any significant accumulation of a bimetallic species because the transmetalation occurs in solution faster than the formation of the bimetallic complex. The products resulting from reactions (I) and (II) were observed as indicated by the blue structures in Schemes 4 and 5.

Reaction with NaBArF. NaBArF was employed to abstract the chloride from R_3PAuCl (R = Me, Ph, ^{t}Bu) but the reactions were complicated by the fact that the formed NaCl could not be removed by filtration. The reactions for all three systems (**A**−**C**) were followed in solution by means of ^{31}P NMR spectroscopy. Low temperature ^{31}P NMR experiments performed in THF-d_8 (see the Supporting Information) showed that the transmetalation process is already occurring at −80 °C, which indicates that the reaction is dramatically accelerated relative to those performed without abstracting agent (about 120 times faster) at room temperature.

Subsequently, the reactions were carried out in the glovebox at a relatively low temperature (−30 °C), while the ^{31}P NMR spectra of the resulting solutions were acquired at room temperature (Figure 6). Determination of the overall yields for the processes turned out to be complicated by the fact that complex **9** plus R_3PAuMe (*R* = Me, Ph, ^{t}Bu) equilibrate with **1** and R_3PAuCl, this process being catalyzed by NaBArF. This was confirmed by adding a stoichiomeric amount of NaBArF to a solution of complex **9** in THF-d_8 and $(^t\text{Bu})_3PAuMe$ (See the Supporting Information).

When a stoichiometric amount of "$Me_3PAu^+BArF^-$"[39] was mixed with **1** at −35 °C in THF-d_8, the reaction occurred within seconds with rapid formation of a black precipitate. The ^{31}P NMR spectrum (Figure 6, A) of the filtered reaction mixture for system **A** revealed a relatively clean distribution of the products resulting from the methyl-transfer processes involved in reaction (I) (Scheme 4): $[(dmpe)PtMe(PMe_3)]^+$ complex **5a** and the species involved in reaction (II): Me_3PAuMe, along with traces of complex (dmpe)PtMeCl (**9**). Complex **9** could presumably be generated from the solvent adduct $[(dmpe)PtMe(THF)]^+$ (7-THF) complex, which is formed *via* reaction channel (II) by chloride trapping. However, since the THF adduct could not be observed under our conditions, we cannot exclude a concerted mechanism involving a nucleophilic attack of chloride on the bimetallic species to generate **9** and Me_3PAuMe. In the system involving "$Me_3PAu^+BArF^-$" and **1** the reaction medium was clean enough to integrate the methyl proton peaks of **5a**, Me_3PAuMe, and **9** to provide an approximate product distribution of 0.64:0.35:0.01 (see the Supporting Information). Additionally, the air-stable $[(dmpe)PtMe(PMe_3)]^+BArF^-$ (**5a**) was isolated from the reaction mixture after purification *via* column chromatography, which provided a relative yield for the process (I) of 52%[40] (Table 3, entry 7). Crystals suitable for X-ray analysis were obtained which confirmed the structure of **5a** (Figure S12, Supporting Information)

In a similar fashion, complex $[(dmpe)PtMe_2]$ (**1**) was reacted with "$Ph_3PAu^+BArF^-$" in THF-d_8 at −30 °C (system **B**). The reaction appeared to be slower than for system **A** since the color changed progressively from colorless to purple and finally led to

dx.doi.org/10.1021/ja110405q | *J. Am. Chem. Soc.* 2011, 133, 8914–8926

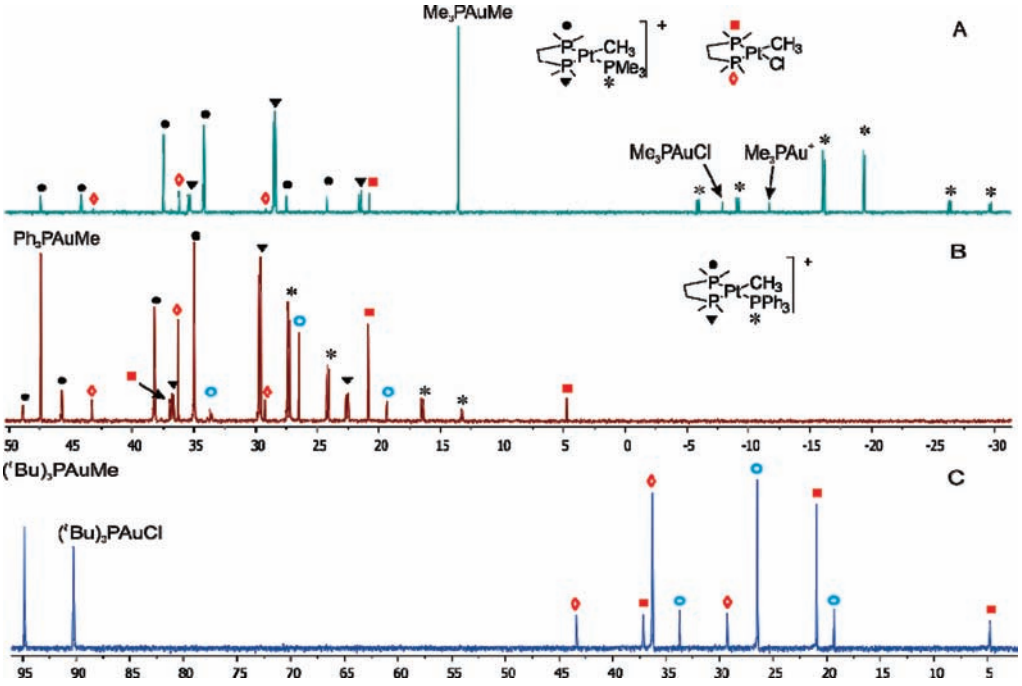

Figure 6. ^{31}P NMR spectra (THF-d_8, 20 °C) of the reactions involving complex **1** (○ in blue) and the cations Me_3PAu^+ (**A**), Ph_3PAu^+ (**B**), and $(^tBu)_3Au^+$ (**C**) generated *in situ,* using NaBArF as halide abstracting agent. The chemical shifts for the transmetalation products of process (I) are marked with ●, ▼, and ∗, while those for reaction process (II) are labeled with and ◊ and ■, both in red, having the R_3PAuMe complexes mentioned in the spectra.

the formation of a black suspension in ∼10 min. After filtration, the observation by ^{31}P NMR (Figure 6, B) of the resulting solution revealed the presence of $[(dmpe)PtMe(PPh_3)]^+BArF^-$ (**5b**) as the major product along with Ph_3PAuMe (singlet at 47.4 ppm), complex **9** and the starting platinum complex **1**. ^{1}H NMR did not allow the determination of a ratio of the transmetalation products since the peaks of Ph_3PAuMe overlap with the Pt-CH_3 signals of **5b** and **1** (see the Supporting Information). However, **5b** was found to be the major reaction product and was isolated from the reaction mixture in 47%,[40] which provided a relative yield for process (I) (Table 3, Entry 8). Crystals suitable for X-ray analysis were also obtained for **5b**, which confirmed the structure of the complex (Figure S12, see the Supporting Information).

When **1** was reacted at room temperature with freshly generated "$(^tBu)_3PAu^+BArF^-$" in THF-d_8 (system **C**), the formation of a black precipitate and the transmetalation product $[(dmpe)PtMeP(^tBu)_3]^+$ (**5c**) were not observed, suggesting that reaction (I) leading to AuMe and **5c** is disfavored in solution. Again the the steric bulk of the tri-(*tert*-butyl)phosphine ligand seems to be responsible for this behavior, as it was in the gas phase. A more detailed inspection of the ^{31}P NMR data (Figure 6C) reveals that only the products resulting from reaction (II) are formed, as observed by the intense singlet peak at 95.3 ppm for $(^tBu)_3PAuMe$ and two singlets at 36.4 and 21.1 ppm for complex **9**, along with unreacted complexes **1** and $(^tBu)_3PAuCl$. Full conversion could not be reached and only 68% of the gold−chloride complex was converted to the gold−methyl complex based on integration of ^{31}P NMR singlet peaks. Attempts to observe the heterobimetallic Pt^{II}/Au^I complex resulting from system **C** failed due to its high reactivity. Evidently the transmetalation process is already taking place at −80 °C, as complexes $(^tBu)_3PAuMe$ and **9** were observed by low temperature ^{31}P NMR (see the Supporting Information).

Reaction with AgOTf. The isolated gold(I) $R_3PAu(NCMe)^+OTf^-$ (R = Me, Ph, ^{t}Bu) cations were slowly added to a precooled (−100 °C) THF-d_8 solution of **1** and the reaction was followed by ^{31}P NMR spectroscopy at −80 °C (Scheme 5, Figure 7).

Mixing **1** with complexes $Me_3PAu(NCMe)^+OTf^-$ or $Ph_3PAu(NCMe)^+OTf^-$, (system **A** and **B**, respectively), generated a dark precipitate even at −100 °C, while in the case of the system **C** ($(^tBu)_3PAu(NCMe)^+OTf^-$) no such decomposition could be observed. We speculate that the decomposition products stem from known reactions of the AuMe formed in process (I) since in system **C** process (I) is shut down. Additionally ethane was detected by ^{1}H NMR for **A** and **B** as the sole hydrocarbon product confirming that a reductive coupling is taking place between gold(I) methyl species leading to ethane and colloidal gold, as had been previously reported.[41−43]

System **A** was the most reactive and ^{31}P NMR of the reaction of complex **1** with $Me_3PAu(NCMe)^+OTf^-$, revealed complete consumption of **1** after 10 min. The major product formed was $[(dmpe)PtMe(PMe_3)]^+$ complex **5a** (Figure 7B), which results from process (I).[44] Moreover, minor peaks stemming from process (II) were observed, i.e. the Me_3PAuMe complex exhibiting a singlet at −13.8 ppm, while two small singlets at 38.1 and 21.2 ppm were observed for cation $[(dmpe)PtMe(NCMe)]^+$ (7-NCMe).[45]

The reaction of cation $Ph_3PAu(NCMe)^+OTf^-$ and complex **1** (system **B**), parallels system **A**, forming products from both process (I): $[(dmpe)PtMe(PPh_3)]^+$ complex **5b**,[44] and process (II): Ph_3PAuMe and complex 7-NCMe. A different product distribution is observed, suggesting that reaction (II) is more favored for system **B** as compared to system **A**; The ^{31}P NMR peaks for both Ph_3PAuMe and 7-NCMe are more intense (Figure 6B) than in system **A**.

dx.doi.org/10.1021/ja110405q | *J. Am. Chem. Soc.* 2011, 133, 8914–8926

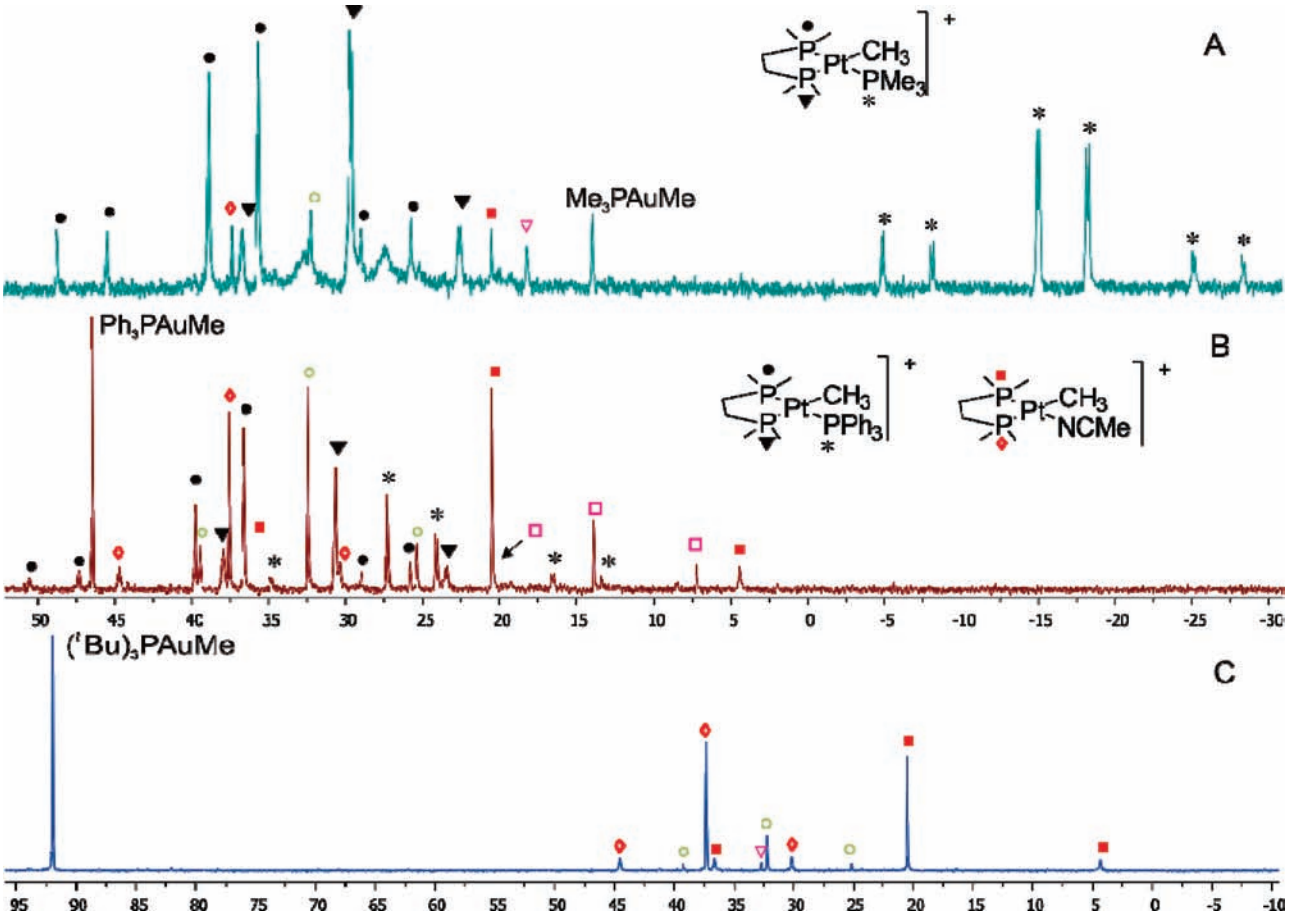

Figure 7. ^{31}P NMR spectra (THF-d_8, −80 °C) of the reactions involving complex **1** and the freshly prepared cations Me_3PAu^+ (**A**), Ph_3PAu^+ (**B**), and $(^tBu)_3Au^+$ (**C**), using AgOTf as halide abstracting agent. The chemical shifts for the transmetalation products resulting from process (I) are marked with ●, ▼, and ∗, while the ones for reaction process (II) are labeled with ◊ (red) and ■ (red), having the R_3PAuMe complexes mentioned in the spectra. Unassigned signals such as at 33.0 ppm ($^1J(P-^{195}Pt)$ = 1715 Hz) (A, B, and C) or at 14.5 ppm ($^1J(P-^{195}Pt)$ = 1619 Hz) (B), and small singlet peaks are marked with ○ (green), □ (purple), and ▽ (purple), respectively.

Finally, complex **1** was mixed with $(^tBu)_3PAu(NCMe)^+OTf^-$ in THF-d_8 at −100 °C to generate the products from system **C**. In contrast to the analogous Pt^{II}/Cu^I bimetallic complex,[5] which could be crystallized at 4 °C, the heterobimetallic complex resulting from system **C** was too reactive to be isolated; the transmetalation products could be observed already at −80 °C after 10 min.

The reaction of the starting compounds **1** and the cationic gold phosphine complex was complete, leading almost exclusively to the products from process (II), $(^tBu)_3PAuMe$ and **7**-NCMe (Figure 6C). The ^{31}P NMR experiments showed also a minor signal which could not yet be assigned; The product involved was too reactive for further characterization.[46]

The high rate of transmetalation reactions in solution may at first appear surprising, considering the barriers measured in the gas phase. However, one has to consider that the uncoordinated products $AuCH_3$ and **7** are likely solvated in solution, causing a strong decrease in the associated barriers. Furthermore, electrostatic interactions of the ion−dipole or ion-induced dipole-type typically lower the energy of gas-phase ion−molecule adducts relative to their dissociation products in solution. The screening of the electrostatic interactions should be treated reasonably by continuum dielectric models of solvation, which would appear in our models as an increase in the energy of the adducts relative to the dissociation limits. Additionally, however, the final dissociations could become associative substitutions in solution, further lowering the associated barriers. An attempt to include solvent effects in our calculations (see the Supporting Information, Figure S14) shows the expected trends, but predicts the transmetalation reactions to be slightly endothermic, in contradiction with their observed irreversibility in solution, although this may simply reflect the limitations of the continuum dielectric solvent models used in the study, which do not include any interactions of individual solvent molecules with the complexes. The relative performance of various DFT methods and solvation models was not investigated further.

■ CONCLUSIONS

We reported the platinum-to-gold methyl transfer to occur in both in gas phase and in solution for three systems. The heterobimetallic complexes **2a**−**c** $\{[(dmpe)PtMe_2]AuPR_3\}^+$ (R = Me (**2a**), Ph (**2b**), ^{t}Bu (**2c**)) could be detected in the gas phase by ESI-MS and the CID reactions of the cations exhibited similar transmetalation reactions. Process (I) leading to $[(dmpe)PtMe(PR_3)]^+$ (R = Me (**5a**), Ph (**5b**)) was observed, while for process (II), complex **7**, $[(dmpe)PtMe]^+$, was generated.

dx.doi.org/10.1021/ja110405q | J. Am. Chem. Soc. 2011, 133, 8914–8926

Gas phase reaction barriers have been measured for heterobimetallic complex **2b** featuring two distinct transmetalation processes, and for **2c**, for which the first pathway is not observed due to the steric demands of the monophosphine.

Truhlar's mPW1K functional in addition to those of the M06 family functional, M06-L and M06-2X, was used to describe the gas-phase mechanisms involved in the transmetalation processes. M06-2X was found to reproduce both observed reaction processes well; its use for these heterobimetallic systems is valid due to the low multireference character as determined by the B_1 parameter.

In solution, low temperature NMR experiments showed that transmetalation reactions are occurring already at −80 °C. Two distinct processes can be observed depending on the monophosphine gold precursor, which involves formation of the observed products **5a**/**b** in reaction (I), while in reaction (II) the solvent-stabilized complex **7**-NCMe or complex **9** along with R_3PAuMe is produced instead of the free coordination site complex **7**. Additionally the transmetalation products **5a** and **5b** from process (I) have been characterized by X-ray diffraction analysis. Interestingly the steric hindrance of the monophosphine supporting ligand on gold can be used to control the transmetalation reaction toward the more interesting process (II) shutting down completely reaction (I), this effect being observed also in the gas-phase experiments.

Our ongoing investigations will focus on the variation of the platinum bidentate ligand and the gold stabilizing ligand, with the aim to combine both Pt-centered C−H activation and transmetalation followed by functionalization.

EXPERIMENTAL SECTION

General Procedures. All the reactions and manipulation were performed under an argon atmosphere using standard Schlenk and glovebox techniques unless stated otherwise. Solvents were distilled under nitrogen over K/Na for hexane, ethyl ether, and tetrahydrofuran and over CaH_2 for acetonitrile and dichloromethane. All deuterated solvents for NMR measurements were degassed via freeze−pump−thaw cycles and stored over activated molecular sieves (4 Å). NMR measurements were recorded on a Varian Mercury XL 300 (^{1}H: 300, ^{31}P: 121 MHz) or Bruker AV400 (^{1}H: 400, ^{31}P: 161 MHz) spectrometers, respectively, with chemical shifts (δ, ppm) reported relative to tetramethylsilane, using residual solvent peaks as internal standard for ^{1}H NMR and 85% H_3PO_4 as an external standard for ^{31}P NMR. Multiplicities are denoted by s (singlet), d (doublet), t (triplet), dd (double doublet), m (multiplet). Elemental analyses were performed at the Mikrolabor of the Laboratorium für Organische Chemie of ETH Zürich. Precursors [(dmpe)PtMe$_2$],[10] Me_3PAuCl,[30] Ph_3PAuCl,[31] (^{t}Bu)$_3$PAuCl[32] as well as compounds Me_3PAuMe,[35] Ph_3PAuMe,[36] and (^{t}Bu)$_3$PAuMe[37] were prepared according to literature procedures. All other starting materials were purchased in reagent grade purity and used without further purification.

[(dmpe)PtMe(PMe$_3$)]$^+$BArF$^-$ (5a). To a cold (−30 °C) solution of **1** (25 mg, 0.066 mmol) in THF-d_8 (0.5 mL) was added a cold filtrated solution of Me_3PAuCl (20 mg, 0.066 mmol) and NaBArF (59 mg, 0.066 mmol) in THF-d_8 (0.5 mL). The resulting solution was stirred at −30 °C for 15 min and at room temperature for 1 h. The resulting black suspension was filtered through a 0.45 μm PTFE syringe filter. ^{31}P NMR spectroscopy of the crude solution showed the presence of **5a**, PMe_3AuMe and some traces of complex **9**. Further purification was achieved by first cooling the THF solution at −30 °C causing all Pt-containing compounds to crystallize. Separation from the unstable Me_3PAuMe complex was realized by filtration. Since **5a** is air- and moisture stable, column chromatography over silica gel using CH_2Cl_2 as eluent yielded 45 mg (52% based on complex **1**) of analytically pure **5a** as a pale-yellow powder. Crystals suitable for X-ray diffraction (XRD) analysis were obtained upon slow concentration of a solution of the complex in dichloromethane. ^{1}H NMR (400 MHz, CD_2Cl_2): δ 7.75 (s, 8H, Ar−*H*), 7.59 (s, 4H, Ar−*H*), 1.91−1.75 (m, 4H, PCH_2CH_2P), 1.64−1.51 (m, 21H, P(CH_3)$_2$ and P(CH_3)$_3$), 0.50 (dd, 3H, ^3J(H−^{31}P) = 14.9 Hz, ^3J(H−^{31}P) = 6.7 Hz, ^2J(H−^{195}Pt) = 58.9 Hz, PtCH_3). ^{31}P{^{1}H} NMR (161 MHz, CD_2Cl_2): δ 34.2 (dd, ^2J(P−P) = 400.7 Hz, ^2J(P−P) = 5.1 Hz, ^1J(P−^{195}Pt) = 2448 kHz, *P*Me$_3$), 26.55 (dd, ^2J(P−P) = 18.8 Hz, ^2J(P−P) = 4.2 Hz, ^1J(P−^{195}Pt) = 1677 Hz, *P*Me$_2$ *trans* to PMe$_3$), −18.8 (dd, ^2J(P−P) = 400.7 Hz, ^2J(P−P) = 19.1 Hz, ^1J(P−^{195}Pt) = 2531 Hz, *P*Me$_2$ *cis* to PMe$_3$). ^{31}P{^{1}H} NMR (121 MHz, THF-d_8): δ 37.9 (dd, ^2J(P−P) = 4.8 Hz, ^2J(P−P) = 397.8 Hz, ^1J(P−^{195}Pt) = 2418 Hz, *P*Me$_3$), 28.6 (dd, ^2J(P−P) = 4.9 Hz, ^2J(P−P) = 18.9 Hz, ^1J(P−^{195}Pt) = 1693 Hz, *P*Me$_2$ *trans* PMe$_3$), −17.7 (dd, ^2J(P−P) = 19.8 Hz, ^2J(P−P) = 397.5 Hz, ^1J(P−^{195}Pt) = 2482 Hz, *P*Me$_2$ *cis* to PMe$_3$).Anal. Calcd for $C_{42}H_{40}BF_{24}P_3Pt$: C, 38.82; H, 3.10. Found: C, 38.91; H, 3.14.

[(dmpe)PtMe(PPh$_3$)]$^+$BArF$^-$ (5b). To a cold (−30 °C) solution of **1** (30 mg, 0.079 mmol) in THF-d_8 was added a cold filtrated solution of Ph_3PAuCl (39 mg, 0.079 mmol) and NaBArF (70 mg, 0.079 mmol) in THF-d_8. The resulting solution was stirred at −30 °C for 15 min and further stirred at room temperature for 1 h. The resulting black suspension was filtered through a 0.45 μm PTFE syringe filter. ^{31}P NMR spectroscopy of the crude filtrate showed the presence of **5b**, Ph_3PAuMe, and [(dmpe)PtMeCl] complex **9**. Following the procedure used for **5a**, analytically pure **5b** was obtained as a white powder (56 mg, 47% base on complex **1**). Crystals suitable for XRD analysis were obtained at 4 °C by layering a concentrated solution of the complex in dichloromethane with hexane. ^{1}H NMR (400 MHz, CD_2Cl_2): δ 7.75 (bs, 8H, Ar−H), 7.58−7.47 (m, 19H, Ar−H), 1.97−1.69 (m, 4H, PCH_2CH_2P), 1.66 (dd, 6H, ^4J(H−^{31}P) = 2.5 Hz, ^2J(H−^{31}P) = 10.5 Hz, ^3J(H−^{195}Pt) = 35.1 Hz, PCH_3), 0.91 (d, 6H, ^2J(H−^{31}P) = 9.2 Hz, ^3J(H−^{195}Pt) = 18.0 Hz PCH_3), 0.50 (dd, 3H, ^3J(H−^{31}P) = 7.0 Hz, ^3J(H−^{31}P) = 13.0 Hz, ^2J(H−^{195}Pt) = 57.5 Hz, PtCH_3). ^{31}P{^{1}H} NMR (161 MHz, CD_2Cl_2): δ 34.4 (dd, ^2J(P−P) = 4.3 Hz,^2J(P−P) = 393.4 Hz, ^1J(P−^{195}Pt) = 2627 Hz, *P*Ph$_3$), 28.1 (dd, ^2J(P−P) = 5.9 Hz, ^2J(P−P) = 17.1 Hz, ^1J(P−^{195}Pt) = 1710 Hz, *P*Me$_2$ *trans* to PPh$_3$), 24.5 (dd, ^2J(P−P) = 16.8 Hz, ^2J(P−P) = 391.8 Hz, ^1J(P−^{195}Pt) = 2689 Hz, *P*Me$_2$ *cis* to PPh$_3$). ^{31}P{^{1}H} NMR (121 MHz, THF-dd_8): δ 36.6 (dd, ^2J(P−P) = 4.4 Hz, ^2J(P−P) = 288.5 Hz, ^1J(P−^{195}Pt) = 2609 Hz, *P*Ph$_3$), 29.7 (dd, ^2J(P−P) = 4.6 Hz, ^2J(P−P) = 16.8 Hz, ^1J(P−^{195}Pt) = 1720 Hz, *P*Me$_2$ *trans* PPh$_3$), 25.7 (dd, ^2J(P−P) = 16.9 Hz, ^2J(P−P) = 388.7 Hz, ^1J(P−^{195}Pt) = 2642 Hz, *P*Me$_2$ *cis* to PPh$_3$).Anal. Calcd for $C_{57}H_{46}BF_{24}P_3Pt$: C, 46.08; H, 3.12. Found: C, 46.18; H, 3.39.

Mass Spectrometry. *Sample Preparation.* Fresh 8 mM stock solutions of [(dmpe)PtMe$_2$] and of R_3PAuCl (R = Me, Ph, ^{t}Bu) in acetonitrile were prepared and stored no longer than two days in a glovebox at −35 °C. Samples for ESI-MS were prepared by adding 10 μL of R_3PAuCl stock solution of to 2 mL precooled (−35 °C) acetonitrile containing 1 mg of NaOTf; after mixing for 5−10 min the solution was filtered through a 0.45 μm PTFE syringe filter. To this solution was then added 10 μL of platinum complex stock solution. The resulting solutions were used immediately after mixing, and the samples were stored during the experiment at −35 °C to prevent possible decomposition.

Mass Spectrometric Measurements. Mass spectra were recorded on a ThermoFinnigan TSQ Quantum instrument. In a drybox, the sample was introduced into a gastight syringe which was taken out and immediately connected to the electrospray source. The solution was electrosprayed using a spray voltage of 5 kV and a transfer capillary temperature of 120 °C (Capillary Offset 10 V). The tube lens voltage was set at 100 V for all measurements. Collision-induced dissociation (CID) spectra were measured at 50 V collision offset with argon (0.2 mTorr) as the collision gas.

CID Threshold Measurements. Energy-resolved CID threshold measurements were performed on a Finnigan MAT TSQ-700 tandem mass spectrometer, customized as described previously.[8c] For the more reactive systems **2a** and **2b** a FlowStart B-200 (part # FCB-200.001) equipped with a microfluid chip reactor was connected to the spray head of our TSQ-700 instrument. The solution of $R_3PAu^+OTf^-$ (R = Me, Ph) and **1** could then be mixed rapidly just before reaching the sray, The FlowStar B-200 is also equipped with a thermocouple connected to a temperature controller (set to −5 °C in our experiment) for mixing of the solution at a desired temperature. The ions were electrosprayed and transferred into a 24-pole ion guide where they were thermalized to 343 K with argon (∼10 mTorr). The ion of interest was mass-selected in the first quadrupole and collided with argon (30−110 μTorr) in the octopole collision cell, and the products were mass-analyzed in the second quadrupole. A retarding potential measurement of the kinetic energy distribution of mass-selected ions was performed before each experiment, yielding Gaussian distributions with fwhm between 1.3 and 1.9 eV in the laboratory frame. The energy dependence of the reactant and product signals were monitored simultaneously and converted to reactive cross sections as described by Ervin et al.[49] To remove multiple-collision effects the data was recorded at several argon pressures, and the cross sections were extrapolated to zero-collision gas pressure. To extract the activation energies, the cross-section data were fitted using our L-CID program.[12] The transition-state parameter was set to tight for the reaction **2b** → **5b** + AuMe, and to lose for **2b** → **7** + Ph_3PAuMe and for **2c** → **7** + $(^tBu)_3PAuMe$. Ancillary methyl groups, phenyls and ^{t}Bu groups bounded to phosphines, as well as PPh_3 and $P(^tBu)_3$ units as a whole, were considered free rotors (totaling 9 for **2b** and 18 for **2c**). For each of the three independent data sets 15 L-CID fits were used to obtain fitted reaction parameters and standard deviations. E_0 values are given in kcal mol^{-1} and the corresponding standard deviations include a 0.15 V laboratory-frame uncertainty.

Computational Methods. Density functional theory (DFT) calculations were performed with the Gaussian 03[50]/09[47] suites of programs as described previously,[5,8a] employing the BP86 exchange-correlation functional for geometry optimization. The Stuttgart/Dresden basis set and effective core potential were used for transition metals along with a 6-31G(d,p) basis set on all other atoms. Because of the flat character of the potential energy surfaces encountered, the GDIIS algorithm was used systematically and tight criteria were imposed for both geometry and SCF convergence. The nature of each stationary point was confirmed by a frequency analysis which also afforded the zero-point energy (ZPE) correction; for the transition states the imaginary vibrational mode corresponded to the expected reaction coordinate. This method was found to accurately reproduce the experimental geometries of complexes **5b** and **5c** obtained in this work, as well as that of the closely related bimetallic cation $\{[(dmpe)PtMe_2]Cu[P(^tBu)_3]\}^+$.[5]

Additionally, density functionals were screened with the Amsterdam Density Functional (ADF2008)[51] suite as follows: the electron density was calculated using the BP86 functional and a TZP basis set without frozen core, and energies were evaluated for 69 density functional using the 'METAGGA' and 'HARTREEFOCK' keywords. Relativistic effects were treated *via* the scalar zeroth-order regular approximation (ZORA) formalism including spin−orbit coupling. The Gaussian BP86/6-31G(d,p);Pt, Au:SDD zero-point energy corrections were added to the energies calculated for mPW1K, M06-L and M06-2X and are presented in Table S5.

■ ASSOCIATED CONTENT

Supporting Information. Experiments details, ESI-MS spectra, threshold-CID measurements, X-ray structures and data for **5a** and **5b**, calculated geometries and single-point energies, evaluation of B_1 parameters for **2a**, DFT evaluation for the nonobserved reactions and NMR data. Complete refs 47 and 50 are available as SI refs 11 and 10, respectively. This material is available free of charge via the Internet at http://pubs.acs.org.

■ AUTHOR INFORMATION

Corresponding Author
peter.chen@org.chem.ethz.ch

■ ACKNOWLEDGMENT

We thank the Swiss National Foundation for support of this work. S.D. thanks Dr. Couzijn E. P. A. for suggestions when writing this manuscript.

■ REFERENCES

(1) (a) de Meijere, A., Diederich, F., Eds. *Metal-Catalyzed Cross-Coupling Reactions*, 2nd ed.; Wiley-VCH: Weinheim, 2004. (b) Billington, D. C. In *Comprehensive Organic Synthesis*; Pattenden, G., Ed.; Pergamon Press: Oxford, 1991; Vol. 3, pp 413−549. (c) Beletskaya, I. P.; Cheprakov, A. V. In *Applications of Coordination Chemistry* ; Ward, M. D., Vol. Ed.; McCleverty, J. A., Meyer, T. J., Eds. in Chief; Comprehensive Coordination Chemistry II, Vol. 9; Elsevier: Amsterdam, Boston, 2003; pp 305−368. (d) Osakada, K.; . In *Current Methods in Inorganic Chemistry*; Kurosawa, H., Yamamoto, A., Eds.; Elsevier Science B.V.: Amsterdam, Boston, 2003; Vol. 3, pp 233−291.

(2) Chinchilla, R.; Najera, C. *Chem. Rev.* **2007**, *107*, 874−922 and references therein.

(3) (a) Stephan, D. W. *Coord. Chem. Rev.* **1989**, *95*, 41–107. (b) Bosnich, B. *Inorg. Chem.* **1999**, *38*, 2554–2562. Wheatley, N.; (c) Kalck, P. *Chem. Rev.* **1999**, *99*, 3379–3419. (d) Santi, S.; Ceccon, A.; Bisello, A.; Durante, C.; Ganis, P.; Orian, L.; Benetollo, F.; Crociani, L. *Organometallics* **2005**, *25*, 4691–4694. (e) Greenwood, B. P.; Forman, S. I.; Rowe, G. T.; Chen, C.-H.; Foxman, B. M.; Thomas, C. M. *Inorg. Chem.* **2009**, *48*, 6251–6260. (f) Shibasaki, M.; Kanai, M.; Matsunaga, S.; Kumagai, N. *Acc. Chem. Res.* **2009**, *42*, 1117–1127. (g) Hashmi, A. S. K.; Lothschütz, C.; Döpp, R.; Rudolph, M.; Ramamurthi, T. D.; Rominger, F. *Angew. Chem., Int. Ed.* **2009**, *48*, 8243–8246. *Angew. Chem.* **2009**, *121*, 8392–8395.

(4) (a) Kuyper, J.; van Vliet, P. I.; Vrieze, K. *J. Organomet. Chem.* **1976**, *105*, 379–387. (b) Kuyper, J.; Vrieze, K. *J. Organomet. Chem.* **1976**, *107*, 129–138. (c) Casalnuovo, A. L.; Laska, T.; Nilsson, P. V.; Olofson, J.; Pignolet, L. H. *Inorg. Chem.* **1985**, *24*, 233–235. (d) Balch, A. L.; Catalano, V. J.; Olmstead, M. M. *Inorg. Chem.* **1990**, *29*, 585–586. (e) Balch, A. L.; Catalano, V. J. *Inorg. Chem.* **1991**, *30*, 1302–1308. (f) Kickham, J. E.; Loeb, S. J. *Organometallics* **1995**, *14*, 3584–3587. (g) Heckenroth, M.; Kluser, E.; Neels, A.; Albrecht, M. *Angew. Chem., Int. Ed.* **2007**, *46*, 6293–6296. (h) Xia, B.-H.; Zhang, H.-X.; Che, C.-M.; Leung, K.-H.; Phillips, D. L.; Zhu, N.; Zhou, Z.-Y. *J. Am. Chem. Soc.* **2003**, *125*, 10362–10374. (i) Ara, I.; Falvello, L. R.; Forniés, J.; Sicilia, V.; Villarroya, P. *Organometallics* **2000**, *19*, 3091–3099. (j) Ara, I.; Forniés, J.; Sicilia, V.; Villarroya, P. *Dalton Trans* **2003**, 4238–4242. (k) Kim, M.; Taylor, T. J.; Gabbaï, F. P. *J. Am. Chem. Soc.* **2008**, *130*, 6332–6333. (l) Yamaguchi, T.; Yamazaki, F.; Ito, T. *J. Am. Chem. Soc.* **1999**, *121*, 7405–7406. (m) Moret, M.-E.; Chen, P. *J. Am. Chem. Soc.* **2009**, *131*, 5675–5690.

(5) Moret, M.-E.; Serra, D.; Bach, A.; Chen, P. *Angew. Chem., Int. Ed.* **2010**, *49*, 2873–2877. *Angew. Chem.* **2010**, *122*, 2935–2939.

(6) Arsenault, G. J.; Anderson, C. M.; Puddephatt, R. J. *Organometallics* **1988**, *7*, 2094–2097.

(7) For reviews: (a) Schröder, D.; Schwarz, H. *Angew. Chem.* **1995**, *107*, 2126–2150. *Angew. Chem., Int. Ed. Engl.* **1995**, *34*, 1973–1995. (b) Plattner, D. A. *Int. J. Mass. Spectrom.* **2001**, *207*, 125–144. (c) Plattner, D. A. *Top. Curr. Chem.* **2003**, *225*, 153–203. (d) Operti, L.; Rabezzana, R. *Mass. Spectrom. Rev.* **2003**, *22*, 407–428. (e) Schwarz, H. *Angew. Chem., Int. Ed.* **2003**, *42*, 4442–4454. *Angew. Chem.* **2003**, *115*, 4580–4593. (f) Böhme, D. K.; Schwarz, H. *Angew. Chem., Int. Ed.*

2005, *44*, 2336–2354. *Angew. Chem.* **2005**, *117*, 2388–2406. (g) Operti, L.; Rabezzana, R. *Mass. Spectrom. Rev.* **2006**, *25*, 483–513. (h) Schröder, D.; Schwarz, H. *Proc. Natl. Acad. Sci. U.S.A.* **2008**, *105*, 18114–18119. (i) Johnson, G. E.; Mitrić, R.; Bonaćić-Koutecký, V.; Castleman, A. W., Jr. *Chem. Phys. Lett.* **2009**, *475*, 1–9. (j) Schlangen, M.; Schwarz, H. *Dalton Trans.* **2009**, 10155–10165. (k) Roithová, J.; Schröder, D. *Chem. Rev.* **2010**, *110*, 1170–1211.

(8) (a) Torker, S.; Merki, D.; Chen, P. *J. Am. Chem. Soc.* **2008**, *130*, 4808–4814. (b) Fedorov, A.; Moret, M.-E.; Chen, P. *J. Am. Chem. Soc.* **2008**, *130*, 8880–8881. (c) Couzijn, E. P. A.; Zocher, E.; Bach, A.; Chen, P. *Chem.—Eur. J.* **2010**, *16*, 5408–5415. (d) Gerdes, G.; Chen, P. *Organometallics* **2003**, *22*, 2217–2225. (e) Moret, M.-E.; Chen, P. *Organometallics* **2007**, *26*, 1523–1530. (f) Batiste, L.; Fedorov, A.; Chen, P. *Chem. Commun.* **2010**, *46*, 3899–3901.

(9) For other examples: (a) Waters, T.; O'Hair, R. A.; Wedd, A. G. *J. Am. Chem. Soc.* **2003**, *125*, 3384–3396. (b) Waters, T.; Khairallah, G. N.; Wimala, S. A. S. Y.; Ang, Y. C.; O'Hair, R. A. J.; Wedd, A. G. *Chem. Commun.* **2006**, 4503–4505. (c) Waters, T.; Wedd, A. G.; O'Hair, R. A. J. *Chem.—Eur. J.* **2007**, *13*, 8818–8829. (d) Gimbert, Y.; Lesagne, D.; Milet, A.; Fournier, F.; Greene, A. E.; Tabet, J.-C. *Org. Lett.* **2003**, *5*, 4073–4075. (e) Thota, R.; Lesage, D.; Gimbert, Y.; Giordano, L.; Humbel, S.; Milet, A.; Buono, G.; Tabet, J.-C. *Organometallics* **2009**, *28*, 2735–2743.

(10) Canty, A. J.; Watson, R. P.; Karpiniec, S. S.; Rodemann, T.; Gardiner, M. G.; Jones, R. C. *Organometallics* **2008**, *27*, 3203–3209.

(11) Cation **7** could in principle also be formed by dissociation of R_3P (R = Me, Ph) from the observed complexes **5a** and **5b**, respectively. The products of such sequential processes would be higher in energy compared to those of reaction (II) by an amount corresponding to the binding energy of R_3P to the MeAu. Thus, the modeling of those processes was not included.

(12) Narancic, S.; Bach, A.; Chen, P. *J. Phys. Chem. A* **2007**, *111*, 7006–7013.

(13) One can argue that the simple appearance of the two channels simultaneously means that reaction (I) and (II) involve either (i) two tight TS models, (i) two loose TS models, or (i) one tight and one loose TS models, respectively. In the first two cases, both thresholds must be similar. The only way to obtain very different thresholds is when the two transition state models are different in nature (tight/loose). In our case channel (I) shows a complicated migration of a ligand and a methyl group, while channel (II) involves a methyl migration, which are both followed by a dissociation step. It is quite plausible then that channel (I) be treated with a tight TS model and channel (II) with a loose one. This is confirmed by DFT calculations.

(14) Both assumptions have been taken into account in our experimental treatment. The L-CID fitting using a tight model, presented in the main article, (Table 1) leading to a barrier of 22.3 kcal mol^{-1}, but also the loose one leading to a barrier of 36.8 kcal mol^{-1}, which is presented in the Supporting Information (Table S2, Figure S9).

(15) Becke, A. D. *Phys. Rev. A* **1988**, *38*, 3098–3100.

(16) Perdew, J. P. *Phys. Rev. B* **1986**, *33*, 8822–8824.

(17) Lynch, B. J.; Fast, P. L.; Harris, M.; Truhlar, D. G. *J. Phys. Chem. A* **2000**, *104*, 4811–4815.

(18) Butschke, B.; Schröder, D.; Schwarz, H. *Organometallics* **2009**, *28*, 4340–4349.

(19) Iron, M. A.; Martin, J. M. L.; Boom, M. E. v. d. *J. Am. Chem. Soc.* **2003**, *125*, 11702–11709.

(20) Iron, M. A.; Lo, H. C.; Martin, J. M. L.; Keinan, E. *J. Am. Chem. Soc.* **2002**, *124*, 7041–7054.

(21) Zhao, Y.; Schultz, N. E.; Truhlar, D. G. *J. Chem. Theory Comput.* **2006**, *2*, 364–382.

(22) Zhao, Y.; Truhlar, D. G. *J. Chem. Phys.* **2006**, *125*, 194101.

(23) Zhao, Y.; Truhlar, D. G. *Acc. Chem. Res.* **2008**, *41*, 157–167.

(24) Zhao, Y.; Truhlar, D. G. *Theor. Chem. Acc.* **2008**, *120*, 215–241.

(25) Zhao, Y.; Schultz, N. E.; Truhlar, D. G. *J. Chem. Theory Comput.* **2006**, *2*, 364−382. Initially proposed for M05-2X density functional.

(26) Schultz, N. E.; Zhao, Y.; Truhlar, D. G. *J. Phys. Chem. A* **2005**, *109*, 4388–4403.

(27) Schultz, N. E.; Zhao, Y.; Truhlar, D. G. *J. Phys. Chem. A* **2005**, *109*, 11127–11143.

(28) Arsenault, G. J.; Anderson, C. M.; Puddephatt, R. J. *Organometallics* **1988**, *7*, 2094–2097.

(29) Puddephatt, R. J.; Thompson, P. J. *J. Chem. Soc., Dalton Trans.* **1975**, 1810–1814.

(30) Isab, A. A.; Fettouhi, M.; Ahmada, S.; Ouahabb, L. *Polyhedron* **2003**, *22*, 1349–1354.

(31) Mezailles, N.; Richard, L.; Gagosz, F. *Org. Lett.* **2005**, *7*, 4133–4136.

(32) Guido, B.; Laura, B. A.; Flavio, B.; Ram, G. G.; Giovanni, M. *Gazz. Chim. Ital.* **1982**, *112*, 539–542.

(33) Peters, R. G.; White, S.; Roddick, D. M. *Organometallics* **1998**, *17*, 4493–4499.

(34) A control experiment in THF-d_8, starting from isolated complexes **9** and $(^tBu)_3PAuMe$ did not show evidence of a reverse transmetalation process even after 4 days of reaction at room temperature. Thus, an equilibrium is not taking place (see the Supporting Information).

(35) Battisti, A.; Bellina, O.; Diversi, P.; Losi, S.; Marcetti, F.; Zanello, P. *Eur. J. Inorg. Chem.* **2007**, *6*, 865–875.

(36) Mizushima, E.; Cui, D.-M.; Nath, D. C. D.; Hayashi, T.; Tanaka, M. *Org. Synth.* **2006**, *83*, 55–60.

(37) Schmidbaur, H.; Aly, A. A. M. *Angew. Chem., Int. Ed.* **1980**, *19*, 71–72. *Angew. Chem.* **1980**, *92*, 66–67.

(38) Other halides abstracting agents were also used, NaOTf and $AgPF_6$. NaOTf was too ineffective in removing all chloride from the gold(I) complexes, which led to insoluble gold precursors at the onset of the reactions, while for $AgPF_6$, fluorine incorpartion reaction was observed leading to complicated mixtures.

(39) A chloride is observed in the final product (**9**) even after filtration, which shows that complete Cl abstraction did not take place. Subsequently, "$R_3PAu^+BArF^-$" will be referred to as a mixture of R_3AuCl and NaBArF).

(40) Based on starting material complex **1**.

(41) Tamaki, A.; Kochi, J. K. *J. Organomet. Chem.* **1973**, *61*, 441–450.

(42) Tamaki, A.; Magennis, J. K.; Kochi, J. K. *J. Am. Chem. Soc.* **1973**, 6487–6488.

(43) Coates, G. E.; Parkin, C. *J. Chem. Soc.* **1963**, 421–429.

(44) We cannot totally rule out that, in solution phase, complexes **5a/b** can also be formed in a consecutive reaction between free monophosphine and the solvent-stabilized **7-THF** or **7-NCMe**. However, peaks corresponding to free phosphine have not been observed during our ^{31}P NMR experiments in solution.

(45) Assignment of complex **7**-NCMe has been confirmed by reacting the known triflate complex [(dmpe)Pt(Me)(OTf)] with acetonitrile, followed by dissolution in THF-d_8. No acetonitrile for THF exchange has been observed (see the Supporting Information).

(46) In system **A**, two broad signals were present at 34.0 and 28 ppm, which is an indication of a fast dynamic behavior. Additionally, two small peaks were observed at 33.0 and 19.1 ppm, the former observed also more clearly for systems **B** and **C**. The presence of platinum satellites ($^1J(P-^{195}Pt)$ = 1715 Hz, Figure 6B and C) for this peak is an indication that this compound is a methyl platinum(II) complex since related complexes [(dmpe)$PtMe_2$] (**1**), [(dmpe)PtMeCl] (**9**), [(dmpe)PtMe(OTf)] and $[(dmpe)PtMe(CH_3CN)]^+$ (**7**-CH_3CN), all exhibit very similar $^{31}P-^{195}Pt$ coupling constants for the phosphine *trans* to the methyl group (1783, 1725, 1789, and 1724 Hz, respectively). Additionally, in system **B** a small unattributed signal has been observed at 14 ppm ($^1J(P-^{195}Pt)$ = 1619 Hz).

(47) Frisch, M. J. et al. *Gaussian 09*, Revision A.1; Gaussian, Inc.: Wallingford CT, 2009. Full reference is provided in Supporting Information as ref 11.

(48) Marenich, A. V.; Cramer, C. J.; Truhlar, D. G. *J. Phys. Chem. B* **2009**, *113*, 6378–6396.

(49) Ervin, K. M.; Armentrout, P. B. *J. Chem. Phys.* **1987**, *83*, 166.
(50) Frisch, M. J. et al. *Gaussian 03*, Revision D.01; Gaussian, Inc.: Wallingford CT, 2004. Full reference is provided in Supporting Information as ref 10.
(51) *ADF*, 2008.01; Science Computing and Modeling, Theoretical Chemistry; Vrije Universiteit: Amsterdam, The Netherlands, http://www.scm.com.